Chapter 2
New Visible-Light Active Semiconductors

Roberto Candal and Azael Martínez-de la Cruz

Abstract So far, the anatase TiO_2 polymorph has been the most studied semiconductor photocatalyst due to its high activity under UV irradiation, high stability against photocorrosion process, and low cost. Nevertheless, from the whole solar energy spectrum that radiates the earth, UV irradiation only represents 4 %. In the same way, other semiconductors such as ZnO, Fe_2O_3, CdS, ZnS, Nb_2O_5, Ta_2O_5, and $BiTaO_4$ have been reported with excellent performance as photocatalysts, among others. In particular, oxides with perovskite structure formed by TaO_6 or NbO_6 octahedra layers have shown the capability to develop an important catalytic activity have reported photocatalytic activity in tantalates and niobates of the type $NaMO_3$ (M = Ta and Nb) for the stoichiometric decomposition of water. In the same way, photocatalytic activity better than TiO_2 has been observed on laminar oxides such as $BaLi_2Ti_6O_{14}$, $MTaO_3$ (M = Li, Na, K), and SrM_2O_7 (M = Nb, Ta) for the degradation of organic pollutants. However, most of these have the same drawbacks that TiO_2 has in relation with their limited range of light absorption and an inefficient charge separation which leads to a high recombination process with the concomitant diminishing of their photocatalytic activity.

For this reason, different alternatives have been proposed to gather the solar energy and then develop large-scale technological applications. Numerous efforts have been made for the development of new visible-light-induced photocatalysts, and some oxides have shown visible-light-driven catalytic activity, such as $In_{1-x}Ni_xTaO_4$, $CaIn_2O_4$, $InVO_4$, $BiVO_4$, and Bi_2MoO_6.

In this chapter, some alternatives to the use of TiO_2 as photocatalyst will be discussed. In Sect. 2.2, the use of semiconductors doped with a transition metal as photocatalysts will be reviewed, in particular the effect of the introduction of metal in the physicochemical properties of semiconductor and in its improvement as

R. Candal
Instituto de Química Física de Materiales, Ambiente y Energía Ciudad Universitaria, Pabellón II, 1428-CABA

Instituto de Investigación e Ingeniería Ambiental Universidad Nacional de San Martín, Campus Miguelete, B1650HMP General San Martín, Buenos Aires, Argentina

A. Martínez-de la Cruz (✉)
Facultad de Ingeniería Mecánica y Eléctrica, Universidad Autónoma de Nuevo León, Av. Universidad s/n, Ciudad Universitaria, San Nicolás de los Garza, N.L. MEXICO, CP 66451
e-mail: azael.martinezdl@uanl.edu.mx

A. Hernández-Ramírez, I. Medina-Ramírez (eds.), *Photocatalytic Semiconductors*,
DOI 10.1007/978-3-319-10999-2_2

photocatalyst. Other interesting possibility in the development of materials with high photocatalytic activity is the doping with nonmetal elements as is discussed in Sect. 2.3. The sensitization of a semiconductor photocatalyst by the action of chemical species allows taking advantage of the free visible-solar energy. This point is included in Sect. 2.4 for the different types of sensitizers.

The association of two or more nanocrystalline semiconductors allows the design of semiconductors heterostructures that are potentially useful in photocatalysis, water splitting, microelectronics, and others. The possibilities of this type of semiconductor coupled photocatalyst are showed in Sect. 2.5. Finally, in Sect. 2.6, the formation of nanostructured semiconductors with photocatalytic activity due to the control of some of their physicochemical properties such as particle size and composition is described.

2.1 Ion-Doped Semiconductors (M^+ = Transition Metal Ion)

The use of semiconductors doped with a transition metal as photocatalysts has been extended in order to improve their physical properties, in particular to induce a narrow energy band gap in its electronic structure. This situation can lead to produce materials with better photocatalytic activity than the well-known TiO_2, in particular to take advantage of the energy that comes from the visible region of the solar spectrum. Some binary and ternary oxides have been proposed in its pristine form, in particular metal transition oxides, as alternative to TiO_2 in the visible region. Nevertheless, the poor photo efficiency in the process of separation of charges under light excitation has limited its future application. To solve this problem, the doped of metal transition oxides with a great variety of transition metal ions represents an interesting expectative, in particular to enhance the photocatalytic properties of the oxide. Additionally, the synthesis of ion-doped semiconductor oxides is easy accomplished and inexpensive and produces large amount of material. The use of wet chemical methods for this purpose, such as coprecipitation, allows the synthesis of materials with specific textural and morphologic properties which can be associated with the photocatalytic activity developed.

The doped of semiconductor oxides for photocatalytic applications included binary oxides such as ZnO, WO_3, Bi_2O_3, and Ta_2O_5 (Bamwenda and Arakawa 2001; Cheng et al. 2007; Hong et al. 2009; Tang et al. 2003) and ternary oxides of the type $BiVO_4$, $InVO_4$, $InTaO_4$, and Bi_2MoO_6 (Kudo et al. 1999; Zhang et al. 2006; Marschall and Wang 2014, Kato et al. 2004), among others. A great variety of synthesis route (see Chap. 3) are used for the synthesis of doped semiconductors which included mainly coprecipitation (Liu et al. 2005), sol–gel (Jaimy et al. 2011), hydrothermal (Jiang et al. 2014), solvothermal (Sun et al. 2013), Pechini method (Wang and Cao 2011), combustion (Ahmad et al. 2013),

microwave (Li et al. 2014a), ultrasound (Omidi et al. 2013), and in the form of thin films by sol–gel (Wang and Cao 2011) deposited by dip coating (Zou et al. 2011).

The binary oxide ZnO with wurtzite structure is one of the most studied photocatalyst after TiO_2 due to its high electrochemical stability and nontoxicity. Several works revealed this oxide as a promising candidate to solve environmental pollution problems related with water purification. Yayapao et al. (2013a) reduced the energy band gap of the oxide by doping the crystal structure with 3 % of Ce by a sonochemical method. The improvement in the activity of Ce-doped ZnO to the photocatalytic degradation of methylene blue in solution was attributed to the presence of a higher concentration of oxygen defects on the surfaces of crystalline-doped material. By the same synthesis route, Yayapao et al. (2013b) prepared Nd-doped ZnO nanoneedles finding the best results for a concentration of 1 % Nd with a performance 2.5 times higher than the undoped ZnO. The origin of this enhancement was the presence of Nd^{3+} ions, which acted as electron scavengers and suppressed the electron–hole recombination.

The sonochemical method was also successfully used for the synthesis of three-dimensional flowerlike Ho-doped ZnO microstructure with improved photocatalytic activity in the degradation of methylene blue (Phuruangrat et al. 2014). The optimum concentration value of Ho^{3+} was established at 3 %, and as was previously described for other lanthanides, the presence of Ho^{3+} prevents the hole-electron recombination due to the ion that acts as an efficient scavenger.

The use of rare earths to doping ZnO also includes europium ions. Europium-doped ZnO hierarchical micro-/nanospheres were synthesized via simple coprecipitation. Eu-doped ZnO was more effective for the degradation of phenol under sunlight irradiation than pure ZnO. This situation was explained on the basis of a better charge separation efficiency and due to hydroxyl radical generation ability as was evidenced by photoluminescence.

Similar successful results were obtained with La^{3+} and Sm^{3+}-doped ZnO materials in the degradation reaction of 4-nitrophenol under UV irradiation (Khatamian et al. 2012).

Although the unfavorable position of E_{CB} is relative to the redox potential of the H_2/H^+, tungsten oxide (WO_3) is a semiconductor oxide of great interest. WO_3 is a material with high stability in aqueous solutions under acidic conditions, it does not undergo photocorrosion process, and it exhibits polymorphism. Indeed, WO_3 has been shown good photocatalytic activity under visible light for degradation of some organic compounds (Takeuchi et al. 2011). Among the polymorphs of WO_3, the phases that have attracted the most attention are the hexagonal (h-WO_3) and monoclinic phase (m-WO_3). The monoclinic phase is an attractive candidate for photocatalytic applications under solar irradiation because it exhibits the proper band-gap energy for the absorption of visible light (Bamwenda and Arakawa 2001; Cheng et al. 2007; Hong et al. 2009).

Different metallic ions such as Mg^{2+}, Al^{3+}, In^{3+}, Fe^{3+}, and Zr^{4+}, among others, have been successfully used to dope the monoclinic crystalline structure of WO_3. The results showed an important change in their photocatalytic properties with

respect to pristine oxide, showing the metallic-doped WO_3 materials better activity than pure WO_3 (Tang et al. 2003). In the same way, the effect of doping with different transition metals (Fe, Co, Ni, Cu, and Zn), at different concentrations, was previously reported for the development of doped WO_3 photocatalysts for splitting of water into hydrogen and oxygen under UV laser irradiation (Hameed et al. 2004). On the other hand, Radecka et al. (2005) have reported an important enhancement in the photoelectrochemical properties of WO_3 when it is doped with Ti ion. This situation was attributed to the fact that Ti^{4+} ions can act as acceptor-type centers in crystalline structure of WO_3 to induce an improvement of light absorption spectra.

Following this line of search, Cheng et al. (2007) have prepared WO_3 and Zn-doped WO_3 thin films on indium-tin oxide glass by a dip coating. Different experimental conditions in the preparation of samples were analyzed, such as Zn (II) concentration, annealing temperature, and number of layers, in order to study the response of the system in the generated photocurrent (Cheng et al. 2007). The photocatalytic activity of the Zn-doped WO_3 was evaluated by using it in a doped photoanode in terms of decay rate of nitrite ions (NO_2^-) under visible light. The best results were obtained with a Zn concentration of 2 %, where an enhancement of both photocurrent and photoactivity of WO_3 was achieved. The authors proposed a photochemical oxidation mechanism where the light absorption is more efficient in Zn-doped WO_3 which allows the production of more photocarriers and consequently the formation of highly active species such as $^{\bullet}OH$ radicals.

The doped of crystalline structure of WO_3 has been extended to rare earth elements. Liu et al. (2007) reported the preparation and photocatalytic activity of dysprosium-doped WO_3 nanoparticles via precipitation. Rhodamine B (rhB) was used as model compound for degradation reaction. They found an important correlation among the photoactivity, photostability, and surface acidity with the adsorbed amount of rhB on the photocatalyst. The mechanism proposed to explain the improvement in the activity of Dy-doped material suggests that doped Dy^{3+} can give an electron to O_2 adsorbed on the surface of doped material to form a superoxide radical ($^{\bullet}O_2^-$) and Dy^{4+}. The Dy^{4+} generated is able to receive a photogenerated electron in the conduction band of WO_3 to form Dy^{3+} inhibiting its recombination with photogenerated holes. This point is reinforced with the fact that Dy-doped WO_3 can enhance the reactivity of rhB on the photocatalyst surface and, therefore, improve its photoactivity.

In the same way, Liu et al. (2005) reported high photoactivity and photostability of Tb-doped WO_3 nanoparticles with respect to pristine WO_3 oxide. WO_3 also was doped with Eu^{3+} with good results from the point of view of photocatalytic applications. Following the Pechini method, Wang and Cao (2011) prepared Eu-doped WO_3 nanoparticles and evaluated its performance as photocatalyst by the degradation reaction of rhB under sunlight-type radiation. Among different physical properties, the authors attributed the improvement of the photocatalytic activity of Eu-doped WO_3 to the distortion of the crystalline structure of the oxide due to the presence of Eu^{3+} ions. The presence of Eu^{3+} ions in the crystalline structure of WO_3 allows an energy band gap of the material ($E_g = 2.65$ eV) suitable to absorb in the visible region of solar spectrum.

The doped of WO_3 with metallic ions also has produced photocatalyst with high performance in the photocatalytic oxidation of water to produce H_2 under UV and visible-light radiation. For this purpose, Zou et al. (2011) reported the microwave synthesis of mesoporous Bi-doped WO_3 materials in presence of cetyltrimethyl ammonium bromine (CTAB) as structure-directing agent. The amount of Bi_2O_3 loading was optimized in a 7.0 wt % for the production of H_2. The incorporation of Bi^{3+} ions seems to avoid the electron–hole pair recombination and can create a visible absorption center and an active surface site.

Another promising example of binary oxide with potential application in photocatalysis and photoelectrocatalysis under visible-light illumination is Bi_2O_3, which can be combined with Nb and doped with different transition metals (Li et al. 2012; Ropero-Vega et al. 2010).

2.2 Nonmetal-Doped Materials

Several semiconductors (SC) with potential applications in photocatalysis, such as ZnO, Ta_2O_5, and Nb_2O_5 (and derived compounds such as niobates and tantalates), are transparent to visible light being activated only with UV (A or B) light. In the case of other colored SC, such as WO_3, Bi_2WO_6, and $BiVO_4$, it is desirable to increase the range of light useful for its activation as photocatalyst. For all these SC, as in the case of TiO_2 discussed in Chap. 1, *nonmetal doping* represents an interesting alternative to improve their photocatalytic performance under visible-light illumination.

The origin of visible-light absorption in these systems can be a consequence of several phenomena. When the energy of the *2p* electronic states of the nonmetal atom and oxygen is similar (as in the case of N in the doping of TiO_2), their mixing possibly leads to the formation of new valence band (vb) with an upward shifted edge that diminishes the band gap energy. However, this is not the only possibility. The nonmetal dopant can also form localized states above the vb, which play an important role in electron transfer to reducible compounds. Other possible explanations are related with oxygen vacancies, color centers, sensitization with nonmetal polymers, and other as shown in Fig. 2.1, adapted from the recently published

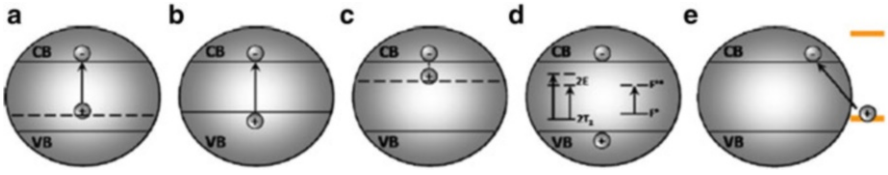

Fig. 2.1 Scheme describing different doping alternatives for SC. (**a**) Localized states above vb. (**b**) Nonmetal-doped SC with narrowed E_g. (**c**) Localized states below CB. (**d**) Color centers formed in the E_g. (**e**) Surface modification with N-containing compounds (From Marshall and Wang, 2014)

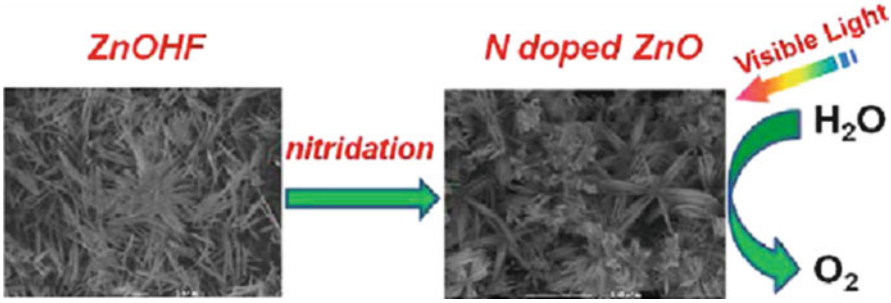

Fig. 2.2 Nitridation of ZnOHF nanobundles led to N-ZnO with similar morphology. This new material displays photocatalytic activity for water splitting under visible light (From Zong et al. 2013. Copyright 2013 American Chemical Society)

review of Marschall and Wang (2014). These authors concluded that homogeneous doping is necessary to shift the absorption edge to visible-light wavelength with band to band excitation, being the amount of dopant related with the threshold of the extended absorption. Homogeneous doping is mostly depending on particle size, crystalline structure, and doping procedure. The type of doping also may depend on the synthesis procedure. In the case of N-TiO_2, Di Valentin et al. (2005), based in DFT theoretical calculations, suggested the existence of two types of N doping: interstitial and substitutional. The first case is favored when calcinations are done under air atmosphere, while the second in the absence of air. Experimental information about the localization of the nonmetal dopant can be obtained by XPS analysis of doped samples prepared under different conditions, as in the work reported by Pulgarin and coworkers (Rengifo-Herrera et al. 2008).

One of the most studied SC other than TiO_2 is ZnO. In spite of its low stability under regular environmental conditions, ZnO is a very attractive material due to its potential applications in disinfection and because of the diversity of shapes in which it can be obtained. An interesting example is represented by N-ZnO nanobundles with visible-light photocatalytic activity, prepared by thermal treatment of ZnOHF nanobundles under NH_3, see Fig. 2.2 (Zong et al. 2013). X-ray photoelectron spectroscopy (XPS) analysis indicated that N was bound to Zn as nitride (Zn-N) and oxynitride (O-Zn-N). The band gap of ZnO was reduced from 2.20 to 1.95 eV as a consequence of substitutional nitrogen doping and the contribution of nitrogen to the top of the vb of ZnO. Water oxidation was performed on this photocatalyst under visible-light ($\lambda > 420$ nm) illumination.

Another nice example is the synthesis of N-doped ZnO mesoporous nanospheres by solvothermal treatment of $Zn(NO_3)_2 \cdot 6H_2O$ in the presence of oleic acid, oleylamine, and octadecene. After heating at 260 °C for 2 h, followed by centrifugation, washing of the solid, and firing at 400 °C, mesoporous ZnO spheres with diameters in the range 100–300 nm were obtained. XPS characterization indicates that N is involved in O-Zn-N bonds. This material displayed enhanced photocatalytic activity for rhodamine degradation under UVA illumination when

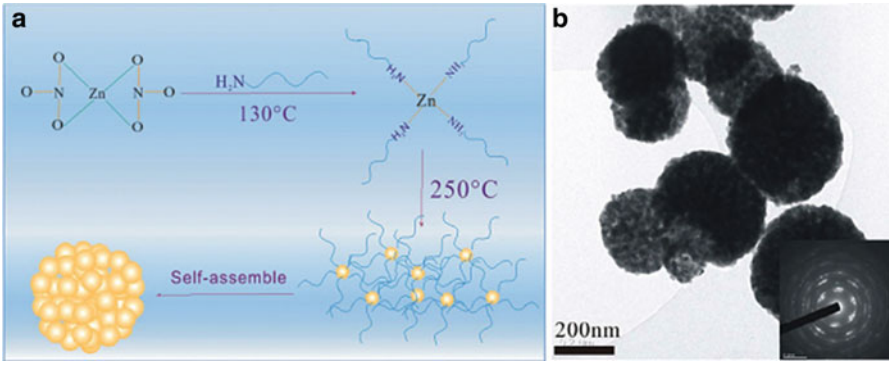

Fig. 2.3 Scheme of the synthesis process (**a**) and TEM image of the N-ZnO mesoporous particles (**b**) (From Zhang et al. 2013)

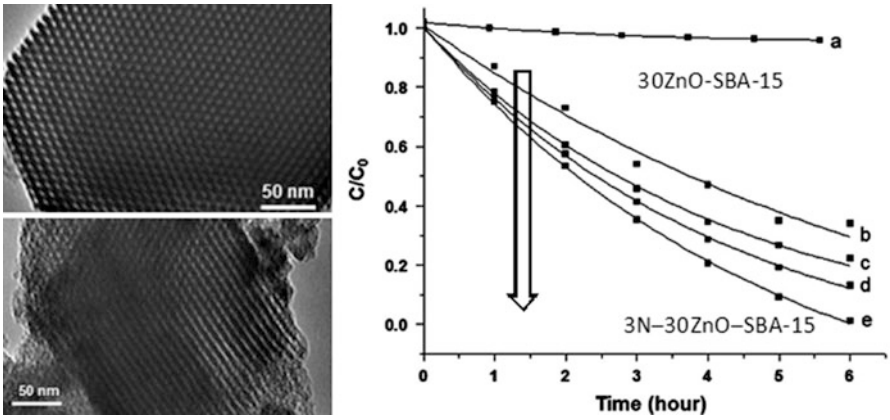

Fig. 2.4 TEM images of SBA-15. (**a**) 3N–30ZnO–SBA-15. (**b**) Photocatalytic degradation of MB under visible-light illumination, using photocatalysts with different level of N doping. The *arrow* indicates the increment in N doping (From Vo et al. 2014)

compared with pure ZnO. Figure 2.3 shows a scheme of the synthetic procedure and TEM images of the obtained particles.

N-ZnO was successfully supported on organized mesoporous silica, in an attempt to develop a photocatalyst with high surface area (Vo et al. 2014). Mesoporous Santa Barbara Amorphous-15 (SBA-15) silica was prepared in the laboratory following well-established procedures and firing at 500°C to remove organics. ZnO was incorporated to SBA-15 by impregnation with $Zn(NO_3)_2$, followed by firing at 550 °C, doping with urea as N source, drying at 100 °C, and annealed at 500 °C. The level of doping was controlled through the repetition of the step involving urea incorporation. The material displayed photocatalytic activity for the discoloration of methylene blue (MB) under visible light. Figure 2.4 shows TEM images of SBA-15 and N-ZnO-SBA-15 and degradation curves of MB.

The materials described before are examples of powdered photocatalysts with potential application in water remediation. Powders can be incorporated to contaminated water producing diluted slurries that can be further exposed to solar or artificial light. Powders are usually more effective than film supported catalyst because the accessibility of the pollutants to the surface of the photocatalyst is not mass transfer limited. However, an important amount of work has been done in the field of N-ZnO films. In most of the cases with applications in photoelectrochemistry, sensors, etc., Wang et al. (2014) have prepared films of N-ZnO by reactive magnetron sputtering. The undoped ZnO films exhibited n-type conduction, while the N-ZnO films showed p-type conduction. XPS analysis of the films indicated that N was involved mostly in Zn-N bonds, substituting O atoms to form NO acceptors in the N-ZnO film. The ZnO:N film has high optical quality and displays the stronger near band edge (NBE) emission in the temperature-dependent photoluminescence spectrum, and the acceptor energy level was estimated to be located 110 meV above the valence band. N-ZnO films were also prepared by other high vacuum techniques, as high vacuum plasma-assisted chemical vapor deposition (HVP-CVD; see, e.g., Barnes et al. 2005) and pulsed-filtered cathodic vacuum arc deposition (PFCVAD; see e.g., Tuzemen et al. 2014). N_2O or N_2 was used as doping agent, respectively. In both cases, as doping level increased, the semiconductor changed from n- to p-type. The stability of the p-type doping depends on the film synthesis. Typically, with aging, the hole conduction decreased and films reverted to n-type conductivity (usually accompanied by an increase in the lattice constant). The films prepared by PFCVAD preserved the p-type doping for at least 12 month.

Tuomisto et al. (2013) prepared N-ZnO films by chemical vapor deposition (CVD) using metallic zinc, NO_2, and NH_3 as precursors. The introduction of N impurities into ZnO films led to the formation of stable vacancy clusters and negative-type defects. N-ZnO and ZnO films prepared by pulsed laser deposition (PLD) were successfully used as platform for the development of biosensors for the determination of uric acid (Jindal et al. 2013). The introduction of defect states upon N doping produced a film with excellent charge transfer characteristics. Besides, doping increased the surface-to-volume ratio providing higher sensitivity to uric acid in comparison with pure ZnO. The exact location of introduced N is unknown, but should be at either substitutional or interstitial sites in the host ZnO lattice. At N low concentrations, due to low formation energy, it is expected to substitute at the O sites improving sensitivity. Sol–gel process, in combination with spin coating technique, was used for the synthesis of Al and N co-doped ZnO. Zinc acetate dihydrate, aluminum nitrate nonahydrate, and ammonium acetate were used as a source for Zn, Al, and N, respectively, in an isopropanol solution with diethanolamine as stabilizer. The spin-coated glass substrates were annealed at 450 °C for 1 h. The optical band gap was reduced from 3.17 to 3.10 due to nitrogen doping. The Al, N co-doped films showed p-type conductivity and high photoelectrical response with a fast recovery of 12 s (Saravanakumar et al. 2013).

Sulfur doping is another approach used to modify the band gap of ZnO. It was reported that sulfur incorporation increases the energy of the vb, while the energy of

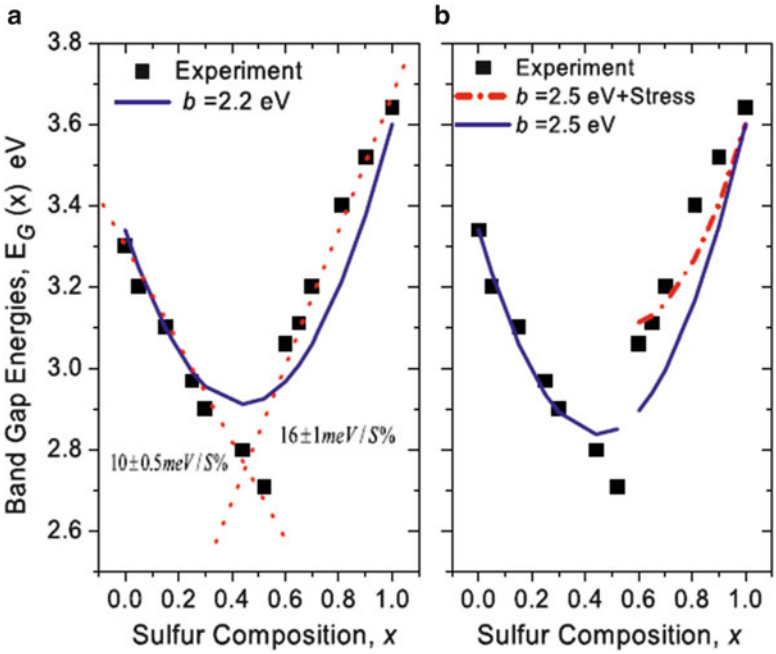

Fig. 2.5 Band gap dependence on the sulfur composition of the $ZnO_{1-x}S_x$ system due to anion substitution with (**a**) $b = 2.2$ eV, (**b**) $b = 2.5$ eV plus stress ($b =$ bowing parameter) (From Thankalekshmi and Rastogi 2012)

the cv remains almost constant (Persson et al. 2006). Electronic states in the band gap are also created. These phenomena lead to the diminution of the band gap energy of ZnO, shifting the absorption of light to the red. Incorporation of sulfur is limited by its low solubility in ZnO and its ZnS phase segregation use to take place at high temperature. To avoid this problem, low temperatures and homogeneously mixed precursors should be used. Films of sulfur-doped ZnO (S-ZnO) were successfully prepared by techniques as pulse laser deposition (Yoo et al. 2002; Xu et al. 2011), reactive sputtering (Meyer et al. 2004), and chemical spray pyrolysis (Thankalekshmi and Rastogi 2012). In the last paper, simple chemicals as $ZnCl_2$ and thiourea dissolved in isopropanol/water 70/30 mixture were used as precursors. When the films deposition was done at 300 °C, the decomposition of zinc(bis) thiourea $Zn[(CS(NH_2)_2]_2Cl_2$) complex occurred concurrently with the decomposition of Zn(OH)Cl (produced by thermolysis of $ZnCl_2.(H_2O)_4$ on the hot substrate) in the presence of ZnO. Under this condition, the incorporation of S at the O sites is highly probable, and alloyed $ZnO_{1-x}S_x$ films were formed without ZnO and ZnS phase separation. XPS analysis confirmed the formation of the mixed film by S^{2-} substitution at the O^{2-} lattice sites. The band gap decreased as the content of S increased from $0 \leq x \leq 0.5$ and increased for higher contents of sulfur (Fig. 2.5). Meyer et al. (2004) reported similar behavior for S-ZnO films prepared by reactive

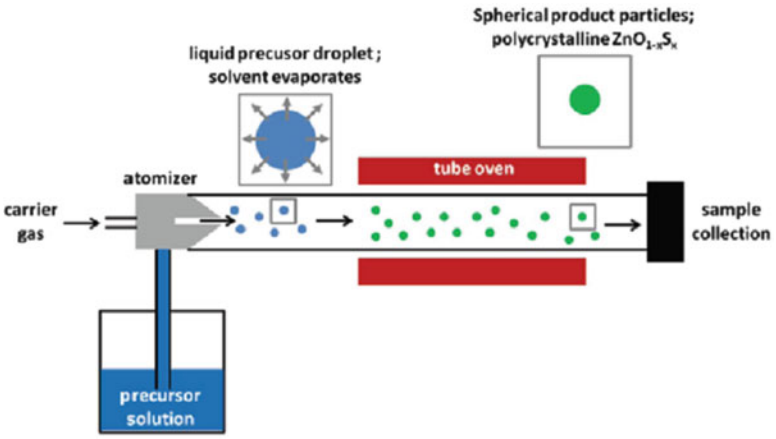

Fig. 2.6 Scheme of the device designed by Leher et al. for the synthesis of ZnO1-xSx spherical particles. The precursor solutions were homogeneous mixtures $[MeZn\text{-}S_{iso}Pr]_8$ and $[MeZnOEtOMe]_4$, in the appropriate proportions, diluted in toluene (From Lehr et al. 2012. Copyright 2012 American Chemical Society)

sputtering. The changes in band gap were approximately fitted by the expression: $E_G(x) = x \cdot E_G(ZnS) + (1-x) \cdot E_G(ZnO)\text{-}b \cdot (1-x) \cdot x + \Delta E_G(\text{stress})$, where $\Delta E_G(\text{stress})$ is the stress-induced shift in the optical transition energy (Thankalekshmi and Rastogi 2012).

S-ZnO films are suitable for applications in electronics, spintronic, photonics, sensors, photoelectrochemistry, etc. But for photocatalytic applications, powders are more versatile than films. Efforts were realized to design synthesis protocols that can produce S-ZnO with different levels of doping in a reproducible way. The strategy followed in these cases was to use homogeneously mixed precursors and relatively low temperatures. Lehr et al. (2012) designed a synthesis that uses organometallic precursors and low temperatures. $[MeZn\text{-}S_{iso}Pr]_8$ was dissolved in $[MeZnOEtOMe]_4$ to prepare solutions in the range $0.5 - 25$ mol % followed by thermolysis at 350 °C. XRD analysis demonstrated that the materials were ZnO doped with different amounts of sulfur. The spectroscopic analysis by diffuse reflectance showed that the band gap shift to the red as the amount of sulfur increased. The band edge was blurred significantly indicating the presence of defect states. A method to prepare spherical particles with diameters in the range 100–200 nm was also developed (see Fig. 2.6). Patil et al. (2010) designed a method based in the mechanochemical synthesis of bisthiourea zinc oxalate (BTZO) powders, followed by thermal treatment at different temperatures. At lower temperatures, the obtained product was ZnS, but as the temperature rose, S-ZnO was produced by controlled oxidation of ZnS. The optimal temperature was 600 °C. The possibility to control the incorporation of sulfur was not reported. The powder displayed enhanced photocatalytic activity for degradation of resorcinol under sunlight when compared with pure ZnO (Patil et al. 2010).

Few other nonmetals were used to dope ZnO. For example, Zheng et al. (2011) reported the synthesis of I-ZnO by a solvothermal method, using zinc salts and iodic acid in polyol medium as precursors. The presence of I in the ZnO network was determined by XRD and EDX analysis. Incident photon to current conversion efficiency (IPCE) analysis of films prepared with ZnO:I showed a red shift, facilitating the utilization of sunlight in the full spectrum range (Zheng et al. 2011).

Tantalum oxide, Ta_2O_5, has also been reported as a semiconductor with applications in photocatalysis. The band gap is in the range 3.9–4.0 eV; thus UV light irradiation is needed for photocatalytic activity. Ta_2O_5-1 % RuO_2 displayed good activity for water splitting under UV irradiation (Sayama and Arakawa 1994). Several attempts were realized in order to shift the absorption of light to the visible part of the solar spectrum. Murase et al. (2004) reported the doping of Ta_2O_5 by thermal treatment under NH_3(g) atmosphere. The incorporation of N was controlled by the heating temperature: $Ta_2O_{5-x}N_x$ with $x = 0.1$, 0.17, 0, 24, and 0.35 were obtained at 600, 620, 650, and 700 °C, respectively. The samples were active for the degradation of 2-propanol in air after long exposure times under visible light (400–530 nm). Very interestingly, by annealing Ta_2O_5 at 850 °C, only TaON was obtained, which absorbed visible light but could not decompose 2-propanol. The synthesis of N-doped Ta_2O_5 by a sol–gel method was recently reported (Ullah et al. 2013). N doping was also produced by annealing under NH_3 atmosphere. The visible and solar light photocatalytic activity of the N-doped material prepared by sol–gel was better than another prepared from commercial Ta_2O_5. The authors reported the conversion of 70 % of toluene under simulated solar light and 30 % of conversion under visible light ($\lambda > 400$ nm). Tantalates and N-doped tantalates were also tested as photocatalyst. $NaTaO_{3-x}N_x$ showed a broad adsorption at 550 nm and was able to decompose gaseous formaldehyde under visible-light illumination (Fu et al. 2008a). It was reported that a high number of lattice defects, obtained with a higher doping, decrease the catalytic activity due to the formation of recombination centers (Fu et al. 2008b; Zhu et al. 2008). Other tantalates, as $InTaO_4$ with perovskite structure and $Sr_2Ta_2O_7$, $Ba_5Ta_4O_{15}$, $CsTaWO_6$ with laminar structure, were doped with nitrogen. In the last cases, the laminar structure helped to reach high levels of doping (Marschall and Wang 2014).

Nb_2O_5 displayed photocatalytic activity for organics oxidation under UV illumination, but not for water splitting. Nitrogen-doped Nb_2O_5 was reported to be able to decompose formaldehyde under visible-light illumination (Murase et al. 2004). N-Nb_2O_5 was compared with N-Ta_2O_5 prepared under identical conditions, for toluene photocatalytic decomposition (Ullah et al. 2013). N-Nb_2O_5 displayed much lower activity than N-Ta_2O_5 due to low amount of defects and inefficient doping. Niobic acid, HNb_3O_8, displays a layered structure which facilitates incorporation of N. N-doped niobic acid was prepared by heating HNb_3O_8 with urea at 400 °C. The obtained material also presented a layered structure; light absorption shifted to the red and displayed enhanced photocatalytic activity for rhodamine B degradation when compared with pure niobic acid (Li et al. 2008).

As was mentioned in Sect. 2.2, WO_3 is a well-known semiconductor with photocatalytic activity. The band gap of WO_3 is in the range 2.4–2.8 eV, so it displays photoactivity with UV–Vis light. Although it is stable toward water oxidation, because the minimum of its conductive band is 0.5 V vs. NHE (more positive than the standard hydrogen potential), water splitting is not possible on WO_3. Interstitial nitrogen doping was found to change the CB position. N_2 placed in the hollow position of WO_3 crystal structure can shift the CB maximum toward more negative values increasing the band gap which, after further interstitial doping, decreases again. The preparation of N_2-WO_3 by thermolysis of ammonium metatungstate under oxygen stream was recently reported (Mi et al. 2012). The optical absorption of N_2-WO_3 was shifted to the red with respect to pure WO_3. Thermal decomposition of ammonium metatungstate can also produce (N^{3-})-doped WO_3 (Takeuchi et al. 2011). This material, after decorated with Pt nanoparticles, exhibited good photocatalytic activity for methanol degradation in gas phase under visible light ($\lambda > 450$ nm).

Tungstates, as Bi_2WO_6, were also doped with nonmetals to improve their photocatalytic activity for organic degradation. Doping with F- modified the surface of the catalyst, leading the reaction mechanism to the *N*-demethylation route (Fu et al. 2008a).

Bismuth vanadates, although they absorb visible light, were also doped with nonmetals to improve photocatalytic activity and to modify reaction mechanism. Such was the case for S-$BiVO_4$ (Zhao et al. 2013) and F-$BiVO_4$ (Liu et al. 2012), respectively. In both cases, the synthesis was carried out by hydrothermal process.

2.3 Dye-Sensitized Semiconductor

The sensitization of a semiconductor has been used for different technological purposes which includes the development of new solar cells (San Esteban and Enriquez 2013), production of hydrogen by water splitting (Li et al. 2014b), and for the degradation of organic dyes coming from industrial effluents (Chatterjee and Dasgupta 2005). In 1991, Grätzel and coworkers developed an efficient dye-sensitized solar cell based in a ruthenium complex adsorbed on nanocrystalline TiO_2 films (O'Regan and Grätzel 1991). This fact opened a new generation of solar cells with higher photon-electron efficiency with a considerable diminishing in the costs of production. In the same way, in recent years, the evolution of hydrogen by water splitting has attracted attention due to the importance of using this gas as energy vector in the future. In this field, the activity of photocatalyst oxides has been considerably improved by its sensitization in order to extend the range in the solar spectrum where it absorbs. Finally, the use of organic-dye/semiconductor-material systems in the process of wastewater treatment via a photosensitization mechanism is a promising field to solve environmental problems.

A great variety of chemical substances have been proposed as effective photosensitizers of a semiconductor. Among these, the most relevant photosensitizers

belong to the families of inorganic sensitizers, coordination metal complexes, and organic dyes with molecular complex structures (Pei and Luan 2012). In the first case, the use of inorganic sensitizers involves semiconductors with narrow band gaps suitable for absorption in the visible region. Among the main physical properties of these compounds are their high stability to photocorrosion process and their absorption in a wide wavelength region. Inorganic sensitizers with considerable performance include metal ions of transition series such as V, Cr, Mn, Fe, and Ni (Chatterjee and Dasgupta 2005) as well as metallic alloys of the type Pt-Au and Au-Ag (Sreethawong and Yoshikawa 2012; Chen et al. 2013). The coordination metal complexes are a type of sensitizers widely used due to their high efficiency to extend the region of absorption of TiO_2; particularly, the ruthenium and osmium complexes have been intensely used for this purpose (Pei and Luan 2012).

An important disadvantage of the sensitization of semiconductor with an organic dye is the gradual decomposition of organic molecule by photocatalytic degradation, due to the natural tendency of organic dyes to undergo redox reactions. In order to solve this problem, the incorporation of electron donors to the reaction medium can be an effective solution, such is the case of EDTA (ethylenediaminetetraacetic acid) (Abe et al. 2004). In the past, numerous organic dyes have been tested with excellent performance to sensitize a semiconductor, in particular TiO_2, such as methyl orange (Liu et al. 2013), methylene blue (Maia et al. 2012), eosin Y (Chen et al. 2013), reactive red 198 (Kaur and Singh 2007), riboflavin (Chu et al. 2007), rose bengal (Whitehead and Hedges 2005), cyanine (Guo et al. 2005), cresyl violet (Dou et al. 2011), hemicyanine (Chen et al. 2005), and merocyanine (Abe et al. 2004). Moreover, some natural organic dyes have been proposed for several reasons. Among others, unlike artificial dyes, the natural ones are available, easy to prepare, low in cost, nontoxic, environmentally friendly, and fully biodegradable (Wongcharee et al. 2007). As an example of this type of compound, some authors have proposed the use of red Sicilian orange juice (*Citrus sinensis*) and the purple extract of eggplant peels (*Solanum melongena*, L.) as natural sensitizers of TiO_2 films for dye-sensitized solar cells (Calogero and Di Marco 2008). In the same way, carotene (Gómez-Ortíz et al. 2010), tannin (Espinosa et al. 2005), and chlorophyll (Kumara et al. 2006) have been utilized also as sensitizers in these devices. Zhou et al. (2011) have reported twenty natural dyes, extracted from natural materials such as flowers, leaves, fruits, traditional Chinese medicines, and beverages, as sensitizers to fabricate dye-sensitized solar cells (DSCs). As main conclusion from the use of natural dyes, they reported that the DSC sensitized by mangosteen pericarp extract offered the highest conversion efficiency of 1.17 % among the 20 extracts. Specifically, the voltage open circuit of mangosteen pericarp extract is comparable to that of the DSC sensitized by a Ru complex N719 (Zhou et al. 2011). An extended review about the use of natural dyes in DSCs has been published by Narayan (2012).

Although the use of organic dyes as sensitizers of semiconductors has the disadvantage of a gradual degradation of organic molecule, at the same time this fact can be used for the photocatalytic degradation of a great variety of organic pollutants from wastewater effluents. Taking advantage of catalytic activity of

semiconductors with high energy band gap, i.e., above $E_g = 3$ eV, the photocatalytic degradation process of organic pollutants can be activated in the visible region of the solar spectrum for environmental applications. The undesirable degradation of the sensitizer in the course of redox reaction applied in devices to produce hydrogen or in a dye-sensitized solar cell can be exploited to remove colored organic pollutants from wastewater.

Nowadays, the industry of synthetic dyes has reached an important place in the development of the society because it supplies its products to a great variety of industries. Usually, these compounds are formed by complex organic molecules with one or more aromatic rings. Unfortunately, about 1–20 % of the total world production of dyes is lost during the dyeing process and is released into the textile effluents (Lopes et al. 2014). Dyehouse wastewater usually contains about 10–50 mg L^{-1} of dyes in solution (Xu et al. 2012). Such concentrations are high enough to induce a remarkable coloring of the receiving water bodies where they are discharged.

The degradation of an organic pollutant by the action of a photocatalyst can take place by two ways. The first of which is by a true photocatalytic process, where radiation on the photocatalyst promotes an electron from its valence band to the conduction band, and then the electron–hole pair is formed. The second possibility is through a photosensitization process, where the radiation excites an electron from the dye and, then, it is injected to the conduction band of the semiconductor oxide. In both processes, a series of consecutive reactions lead to the eventual mineralization of organic dyes to CO_2 and H_2O.

The photosensitization process by rhodamine B (rhB) is well known for different systems (Takizawa et al. 1978) and can be described in the case of a semiconductor oxide (SM) as follows:

$$\mathrm{rhB\ (ads)\ +\ h\nu\ (554\,nm)\ \rightarrow\ rhB^{*}\ (ads)\ (1)\ excitation\ of\ dye} \tag{2.1}$$

$$\mathrm{rhB^{*}\ (ads)\ +\ SM \rightarrow rhB^{\bullet +}(ads)\ +\ SM\ (e_{cb}^{-})\ (2)\ electron\ injection} \tag{2.2}$$

$$\mathrm{SM\ (e_{cb}^{-})\ +\ O_2\ \rightarrow\ SM\ (2)\ +\ O_2^{\bullet -}(3)\ electron\ scavenging} \tag{2.3}$$

$$\mathrm{rhB^{\bullet +}(ads)\ +\ O_2^{\bullet -}\ \rightarrow\rightarrow\rightarrow\ CO_2\ +\ H_2O\ (mineralization\ process)} \tag{2.4}$$

Of course, in order to reach a complete mineralization of the dye, it is necessary that a direct activation of SM by light irradiation occurs too.

$$\mathrm{SM\ (e_{cb}^{-})\ +\ O_2^{\bullet -}\ +\ H^{+}\ \rightarrow HO_2^{-}\ +\ SM} \tag{2.5}$$

$$\mathrm{HO_2^{-}\ +\ H^{+}\ \rightarrow\ H_2O_2} \tag{2.6}$$

$$\mathrm{H_2O_2\ +\ e^{-} \rightarrow {}^{\bullet}OH\ +\ OH^{-}} \tag{2.7}$$

$$\mathrm{rhB^{\bullet +}(ads)\ +\ {}^{\bullet}OH \rightarrow\rightarrow\rightarrow\ CO_2\ +\ H_2O} \tag{2.8}$$

2.4 Coupled Semiconductors

The association of two or more nanocrystalline semiconductors allows the design of semiconductors heterostructures that are potentially useful in photocatalysis, water splitting, microelectronics, and others (Kamat 1997; Beydoun et al. 1999). The advantage of using associations of semiconductors is twofold: (1) to extend the photoresponse by coupling a large band gap semiconductor with a short band gap semiconductor and (2) to retard the recombination of photogenerated charge carriers by injecting electrons into the lower lying conduction band of the large band-gap semiconductor.

There are two principal configurations: coupled and capped semiconductors heterostructures. The principle of charge separation in both structures is displayed in Fig. 2.7a, b.

While the mechanism of charge separation in coupled and capped semiconductors is similar, the interfacial charge transfer is notably different. In a coupled semiconductor system, the particles are in contact with each other and the holes and electrons are available for oxidation or reduction reactions on the surface of different particles. In capped semiconductors with a core shell structure, a charge rectification takes place, and only one of the charge carriers is accessible at the surface; the other charge carrier gets trapped inside the inner semiconductor (Fig. 2.7).

Coupled semiconductors can be prepared by combining colloid systems avoiding heterocoagulation. Nanostructure films of SnO_2/TiO_2 were prepared by deposition of SnO_2 water-based sol on conductive glass followed by deposition of a TiO_2 sol. The coupling of these two wide band gap semiconductors allowed a better charge separation. The CB of SnO_2 (0.0 V vs NHE at pH 7) is more positive than that of TiO_2 (−0.5 V vs NHE at pH 7) and can trap the photogenerated electron. On the other hand, the holes move to the opposite direction and accumulate on TiO_2 particles improving charge separation. This system displayed enhanced photocatalytic activity for acid orange 7 (Vinodgopal and Kamat 1995). In the same direction, the coupling of ZnO with SnO_2 resulted in an improvement of the photocatalytic efficiency of SnO_2 under UV illumination for the degradation of eosin Y (Tanasa et al. 2013).

By coupling small band gap semiconductors with large band gap semiconductors, it is possible to get hole-electron separation using longer wavelength. In the case of CdS/TiO_2, photocurrent generation was observed in the 400–600 nm range. The photogenerated electrons can be injected from CdS to TiO_2 particles, while the holes remain in the CdS particles (Kohtani et al. 1993). The synthesis by chemical route of self-assembled flowerlike CdS/ZnO nanocomposites was recently reported (Jana et al. 2014). Using this coupled system as photocatalyst, the photodegradation of rhodamine B in aqueous solution was enhanced, thanks to the efficiency of the coupled charge transfer mechanism. Figure 2.8 shows a scheme of the process and the synthesized particles. A ternary system containing Ag-ZnO-CdO was prepared by a coprecipitation method. The system was formed by hexagonal plate-like ZnO

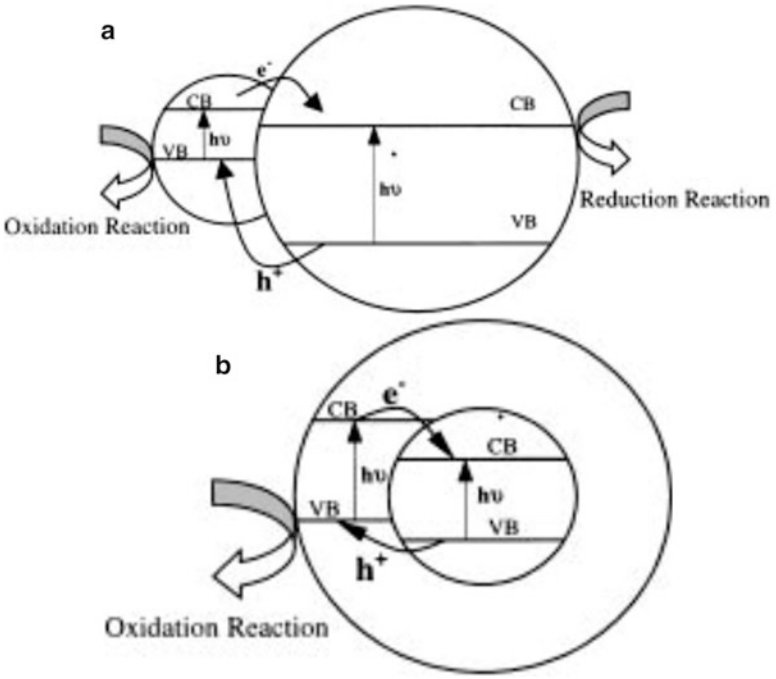

Fig. 2.7 Photoinduced charge separation in semiconductor structure: (**a**) coupled; (**b**) capped semiconductor nanocrystallites (From Beydoun et al. 1999)

structures, containing CdO and Ag clusters on its smooth surfaces. This system had an increased adsorption in the UV and visible region than ZnO prepared in similar way and displayed enhanced photocatalytic activity for the degradation of acid black 1 and acid violet 7 under sunlight (Balachandran et al. 2014).

Another ternary composite was successfully prepared by loading ZnO and CdS nanoparticles in graphene sheets via a one-step hydrothermal method. Photoelectrochemical experiments revealed that the ternary CdS/ZnO/graphene composite exhibits enhanced photocatalytic activity compared with the matrix binary composites and pure ZnO and CdS (Han et al. 2014). Mixed oxide coupled with oxide also shows some improved properties. ZnO-$ZnWO_4$ nanocomposites prepared by sol–gel method displayed higher photoactivity for the degradation of 4-nitrophenol than ZnO and $ZnWO_4$. The high efficiency of the mixed samples was likely due to an improved charge separation as consequence of the relative values of their conduction and valence bands, as shown in Fig. 2.9 (Hamrouni et al. 2014). The coupling of graphene with $BiFeO_3$ also displays photocatalytic enhanced properties under visible-light illumination. The coupling between $BiFeO_3$ nanoparticles and graphene was probably achieved by the formation of Fe-O-C bonds, as determined by XPS and Raman analysis (Li et al. 2014c).

The preparation of capped semiconductors involves the synthesis of the inner core semiconductor colloid of desire size, followed by the controlled deposition of a

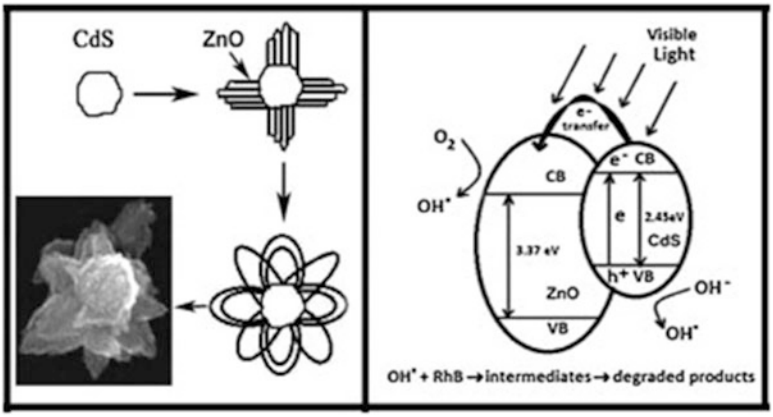

Fig. 2.8 Scheme showing the structure of the flower-shaped particles and the charge transfer process between the coupled semiconductors (From Jana et al. 2014)

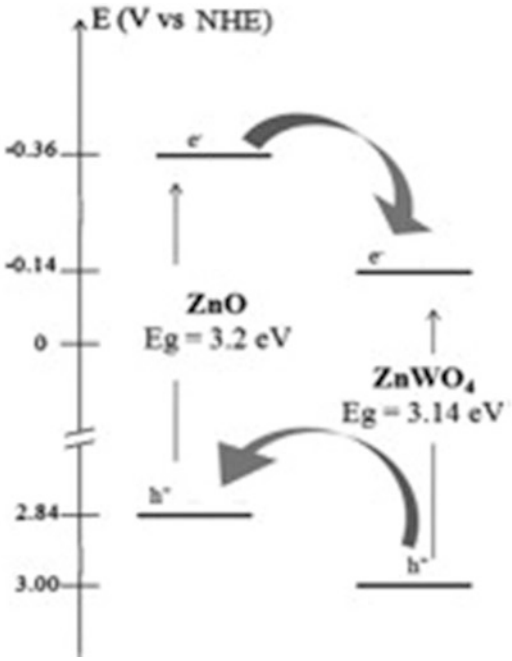

Fig. 2.9 Energy level diagram showing the direction of electron and hole transfer in $ZnO/ZnWO_4$ system (From Hamrouni et al. 2014)

second semiconductor layer. For example, for the synthesis of $TiO_2@SnO_2$, titanium isopropoxide was added dropwise to a SnO_2 water-based colloidal suspension. As the particles became coated with TiO_2, a precipitate containing the capped particles settled down. The thickness of the TiO_2 layer could be controlled through the total amount of added titanium isopropoxide. Due to the electronic band structure, upon UV excitation, the photogenerated electrons accumulate at an

inner core of SnO_2, while holes accumulate at the TiO_2 surface. The holes can be rapidly scavenge away by easily oxidizable species like adsorbed I^- anions. The relative quantum efficiency for I^- oxidation at SnO_2@TiO_2 was two to three times higher than SiO_2@TiO_2 or TiO_2 alone (Kamat 1997).

Although the use of capped and coupled semiconductors present interesting and promising properties that may enhance the photocatalytic efficiency of these systems when compared with the parent semiconductors, it should be considered that the accumulation of holes or electrons may lead to the photocorrosion of one or both materials. Photocorrosion is a major concern when working with potentially toxic materials such as CdS and CdO, which can release soluble species to water. These materials should be carefully tested before using them as photocatalysts.

2.5 Nanostructured Semiconductors: Effect of Size and Composition

Since the discovery of heterogeneous photocatalysis (Honda and Fujishima 1972), numerous efforts have been carried out to understand the mechanism of reaction and how to select the main variables that affect its efficiency. Several authors have associated the efficiency of a semiconductor photocatalyst with electronic, structural, and morphological properties of the material such as the band-gap energy (E_g), crystalline structure, surface area, and morphology. The possibility of controlling these variables is very interesting from a technological point of view because the development of materials with high photocatalytic activity allows their application to environmental fields such as wastewater treatment (Malato et al. 2009).

In the search of semiconductor materials with photocatalytic activity under visible-light irradiation, important efforts have been carried out in the last decade. For example, the TiO_2 anatase polymorph has been doped with nitrogen in order to increase its absorption in the visible range (Yang and Gao 2004). This limitation has attracted the synthesis of new visible-light-driven photocatalysts in recent years. Some compounds such as Bi_2O_3, WO_3, Ag_3VO_4, Bi_2WO_6, and $BiVO_4$ have been recently studied because they have shown visible-light-driven catalytic activity (Eberl and Kisch 2008; Kominami et al. 2003; Konta et al. 2003; Shang et al. 2008; García-Pérez et al. 2012).

In this sense, the search of new photocatalysts with an important improvement in its photocatalytic activity has been focused in the synthesis of semiconductors for a great variety of chemical methods. For semiconductor oxides such as ZnO, $BiVO_4$, and $PbMoO_4$, several experimental methods were reported to prepare the materials with specific morphological and textural properties. The use of wet chemical methods, such as sol–gel, coprecipitation, hydrothermal, microwave, and sonochemical in the presence or absence of organic additives, has been reported as a successful way to develop nanostructured semiconductors. Frequently, the

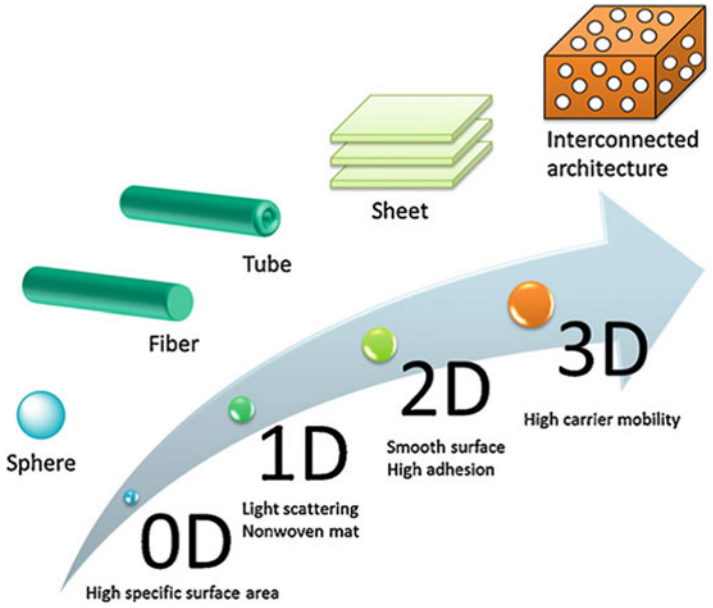

Fig. 2.10 Dimensionality of TiO_2 nanostructure related with the photocatalytic activity of the material. Taken from Nakata and Fujishima (2012)

solid-state reaction method employed to obtain the solid compounds leads to materials with poor photocatalytic activity due to the small surface area developed. The so-called soft chemistry methods have shown to be efficient to prepare better catalysts than those synthesized by classical methods.

The development of nanostructured semiconductors for catalytic applications provides materials with a high value in their surface/volume ratio, but maintaining the physical properties of the bulk material and at the same time including new physical properties due to the relation between surface and volume of the material (Anta 2012). In particular, due to small size of the particles, quantum effect affects directly some physical properties of material such as optical and electronic properties (Nozik et al. 2010). Such situation has opened numerous field of technological application of these materials, which include the development of new generations of solar cells, production of hydrogen, and elimination of pollutants from wastewaters.

From a point of view of photocatalytic applications, the small size of particles of nanostructured semiconductors plays an important role in the activity of photocatalysts. As is well known, the critical step in the heterogeneous photocatalysis is the undesirable recombination of pair electron–hole before they reach the catalyst surface. In this sense, the small size of prepared particles reduces the pathway from the site of generation of the pair electron–hole to the catalyst surface, as is shown in Fig. 2.10.

Among semiconductors with high activity, the anatase polymorph of TiO_2 is the compound most extensively synthesized in nanoscale size. In an interesting review, Nakata and Fujishima (2012) describe how the dimensionality of TiO_2 nanostructures affects its physical properties such as surface area, adsorption, reflectance, adhesion, and carrier transportation properties. They reviewed the formation of TiO_2 nanostructures with different shapes, which include spheres (Chen et al. 2011), nanorods (Yun et al. 2009), fibers (Cheng et al. 2010), tubes (Yu et al. 2010), sheets (Aoyama et al. 2012), and interconnected architectures (Hasegawa et al. 2011). In particular, the dimensionality of TiO_2 nanostructure can be related to the photocatalytic activity of the material, as can be shown in Fig. 2.10.

For example, a higher surface area is desirable in a heterogeneous catalyst, in order to get a higher concentration of active sites where a molecule of pollutant can be anchored to undergo its decomposition by interchange of carriers coming from excitation of semiconductor. To reach this condition, TiO_2 nanostructured with zero dimensionality due to the shape of sphere of its particles can be developed. On the other hand, the development of one-dimensional fiber or nanotube structures promotes a less recombination of pair hole-electron due to the short distance between the place of its generation and the surface of material where pollutant species react. The application of nanostructured TiO_2 for wastewater treatment usually includes the elimination of organic compounds with large and complex molecular structure. For this reason, steric effects in the adsorption of molecules of organic pollutants over the surface of photocatalyst should be taken into account. In these sense, two-dimensional nanosheets have smooth surfaces which leads to a high adhesion of organic molecule. Finally, the presence of channels interconnected in three-dimensional structures promotes a high mobility of carriers to reach the surface of photocatalyst and, then, induce oxidation or reduction reactions.

Zhang et al. (2014) have prepared nanostructured TiO_2 hollow fiber photocatalytic membranes via a facile spinning-sintering method. The photocatalytic activity, permeability, and separation efficiency of the membranes were evaluated using both acid orange 7 and raw sewage as pollutants. For a series of prepared TiO_2 membranes, the calcination temperature was the factor that ruled the photocatalytic activity. This fact had a direct relation with the physical properties of the samples, including the morphology and crystal phase.

Nano-sized TiO_2 for photocatalytic applications also have been synthesized by solvothermal methods under supercritical conditions (Wang et al. 2013). Nanostructured TiO_2 samples were prepared by using a mixture of tetrabutyl orthotitanate (TBOT) and ethanol in supercritical CO_2. The photocatalytic activity of the samples tested with methyl orange was strongly influenced by its corresponding morphology. In particular, the activity of the samples decreased with the increasing particle size.

The synthesis of nanostructures of TiO_2 has been successfully applied for photocatalytic coatings for corrosion protection and surface repair (He et al. 2013). These were developed by the incorporation of a corrosion inhibitor, 8-hydroxyquinoline (8-HQ), into TiO_2 nanoparticles.

The formation of nanostructures has been extended to materials with good performance to absorb in the region visible of solar spectrum. Min et al. have reported the synthesis of nanostructured ZnO/Bi_2WO_6 heterojunction for photocatalytic applications (Min et al. 2012). The formation of this type of heterojunction nanostructure promotes an efficient charge separation and consequently an important improvement of the photocatalytic activity of the material with respect to the pristine oxides.

In the same way, nanostructured WO_3/Bi_2WO_6 heterojunction was prepared by one-step hydrothermal method with high visible-light photocatalytic activity for degradation of rhodamine B (Gui et al. 2012).

Concluding Remarks

The number of pure and doped metal oxide semiconductors available for photocatalysis and other applications that use UV or visible light as a source of energy had notably increased during the last ten years. The force that drives this situation is the need to systematically count hydrogen production or pollution control based on the use of solar energy.

The most studied SC oxides with photocatalytic activity other than TiO_2 are ZnO, WO_3, Ta_2O_5, Nb_2O_5, Bi_2O_3, CdO, and SnO_2. Ternary systems such as bismutates, vanadates, molybdates, and niobates are being increasingly prepared and studied for photocatalytic applications in both pristine and doped form. The great development in SC metal oxide was helped by the advances in wet chemistry synthesis that allows the production of nanostructured powders and films in a relatively economic way. Not only composition can be controlled by an appropriate synthesis design but also the shape, size, and dimensionality of the particles that constitute the powders or the films. Nanostructured materials (powders or films) are essential to reach photoefficiencies higher enough to be applied in industrial processes. The dimensionality of the particles also has a crucial role in the mobility of charge carriers.

Different strategies were used to shift the absorption spectrum to longer wavelength with different results. In some cases, the doping with metal ion was very successful, but in others hole-electron recombination was increased, with a diminution in photocatalytic efficiency. Nonmetal doping increases the absorption of visible light, but the oxidation power of the photogenerated holes is lower than when the system is illuminated by UV light. Sensitization with dyes is successful in the use of visible light, but the dyes are finally degraded after long-term illumination, which suggest that is a good method to eliminate colored pollutants but not very useful for hydrogen production or energy conversion. Coupling of SC is a very interesting possibility, but care should be taken to avoid photocorrosion and dissolution of toxic metals into water. At present, there is not a unique strategy that works for all the systems.

(continued)

(continued)

Each case should be analyzed to find the best approach to improve the use of solar light for water or air remediation, hydrogen production, or energy conversion.

The general trend indicates an improvement in the development of SC materials with high photocatalytic efficiency under visible-light illumination and a better understanding of the physicochemical processes involved in photocatalysis. This knowledge will undoubtedly help to increase the photoefficiency of the new materials that will be designed in the near future.

References

Abe R, Sayama K, Arakawa H (2004) Dye-sensitized photocatalysts for efficient hydrogen production from aqueous I^- solution under visible light irradiation. J Photochem Photobiol A 166:115–122

Ahmad M, Ahmed E, Zhang Y, Khalid NR, Xu J, Ullah M, Hong Z (2013) Preparation of highly efficient Al-doped ZnO photocatalyst by combustion synthesis. Curr Appl Phys 13:697–704

Anta JA (2012) Electron transport in nanostructured metal-oxide semiconductors. Curr Opin Colloid Interface Sci 17:124–131

Aoyama Y, Oaki Y, Ise R, Imai H (2012) Mesocrystal nanosheet of rutile TiO_2 and its reaction selectivity as a photocatalyst. Cryst Eng Comm 14:1405–1411

Balachandran S, Praveen SG, Velmurugan R, Swaminathan M (2014) Facile fabrication of highly efficient, reusable heterostructured Ag–ZnO–CdO and its twin applications of dye degradation under natural sunlight and self-cleaning. RSC Adv 4:4353–4362

Bamwenda GR, Arakawa H (2001) The visible light induced photocatalytic activity of tungsten trioxide powders. Appl Catal A 210:181–191

Barnes TM, Olson K, Wolden CA (2005) On the formation and stability of p-type conductivity in nitrogen-doped zinc oxide. Appl Phys Lett 86:112112

Beydoun D, Amal R, Low G, McEvoy S (1999) Role of nanoparticles in photocatalysis. J Nanopart Res 1:439–458

Calogero G, Di Marco G (2008) Red Sicilian orange and purple eggplant fruits as natural sensitizers for dye-sensitized solar cells. Sol Energy Mater Sol Cells 92:1341–1346

Chatterjee D, Dasgupta S (2005) Visible light induced photocatalytic degradation of organic pollutants. J Photochem Photobiol C 6:186–205

Chen YS, Li C, Zeng ZH, Wang WB, Wang XS, Zhang BW (2005) Efficient electron injection due to a special adsorbing group's combination of carboxyl and hydroxyl: dye-sensitized solar cells based on new hemicyanine dyes. J Mater Chem 15:1654–1661

Chen JS, Chen C, Liu J, Xu R, Qiao SZ, Lou XW (2011) Ellipsoidal hollow nanostructures assembled from anatase TiO_2 nanosheets as a magnetically separable photocatalyst. Chem Commun 47:2631–2633

Chen L, Tran TTT, Huang C, Li J, Yuan L, Cai Q (2013) Synthesis and photocatalytic application of Au/Ag nanoparticle-sensitized ZnO films. Appl Surf Sci 273:82–88

Cheng XF, Leng WH, Liu DP, Zhang JQ, Cao CN (2007) Enhanced photoelectrocatalytic performance of Zn-doped WO_3 photocatalysts for nitrite ions degradation under visible light. Chemosphere 68:1976–1984

Cheng Y, Huang W, Zhang Y, Zhu L, Liu Y, Fan X, Cao X (2010) Preparation of TiO_2 hollow nanofibers by electrospinning combined with sol-gel process. Cryst Eng Comm 12:2256–2260

Chu W, Chan KH, Jafvert CT, Chan YS (2007) Removal of phenylurea herbicide monuron via riboflavin-mediated photosensitization. Chemosphere 69:177–183

Di Valentin C, Pacchioni G, Selloni A, Livraghi S, Giamello E (2005) Characterization of paramagnetic species in N-doped TiO_2 powders by EPR spectroscopy and DFT calculations. J Phys Chem B 109:11414–11419

Dou C, Wen P, Kong X, Nakanishi S, Feng Q (2011) The nonlinear refraction sign turned to reverse by intercalating cresyl violent dye into layered titanate nanosheets. Opt Commun 284:1067–1071

Eberl J, Kisch H (2008) Visible light photo-oxidations in the presence of α-Bi_2O_3. Photochem Photobiol Sci 7:1400–1406

Espinosa R, Zumeta I, Santana JL, Martínez-Luzardo F, González B, Docteur S, Vigil E (2005) Nanocrystalline TiO_2 photosensitized with natural polymers with enhanced efficiency from 400 to 600 nm. Sol Energ Mat Sol C 85:359–369

Fu H, Zhang S, Xu T, Zhu Y, Chen J (2008a) Photocatalytic degradation of RhB by fluorinated Bi_2WO_6 and distribution of the intermediate products. Environ Sci Technol 42:2085–2091

Fu H, Zhang S, Zhang L, Zhu Y (2008b) Visible-light-driven $NaTaO_{3-x}N_x$ catalyst prepared by a hydrothermal process. Mater Res Bull 43:864–872

García-Pérez UM, Sepúlveda-Guzmán S, Martínez-de la Cruz A (2012) Nanostructured $BiVO_4$ photocatalysts synthesized via a polymer-assisted coprecipitation method and their photocatalytic properties under visible-light irradiation. Solid State Sci 14:293–298

Gómez-Ortíz NM, Vázquez-Maldonado IA, Pérez-Espadas AR, Mena-Rejón GJ, Azamar-Barrios JA, Oskam G (2010) Dye-sensitized solar cells with natural dyes extracted from achiote seeds. Sol Energ Mat Sol C 94:40–44

Gui MS, Zhang WD, Chang YQ, Yu YX (2012) One-step hydrothermal preparation strategy for nanostructured WO_3/Bi_2WO_6 heterojunction with high visible light photocatalytic activity. Chem Eng J 197:283–288

Guo M, Diao P, Ren YJ, Meng F, Tian H, Cai SM (2005) Photoelectrochemical studies of nanocrystalline TiO_2 co-sensitized by novel cyanine dyes. Sol Energy Mater Sol Cells 88:23–35

Hameed A, Gondal MA, Yamani ZH (2004) Effect of transition metal doping on photocatalytic activity of WO_3 for water splitting under laser illumination: role of 3d-orbitals. Catal Commun 5:715–719

Hamrouni A, Moussa N, Di Paola A, Parrino F, Houas A, Palmisano L (2014) Characterization and photoactivity of coupled ZnO–$ZnWO_4$ catalysts prepared by a sol-gel method. Appl Catal B Environ 154–155:379–385

Han W, Ren L, Qi X, Liu Y, Wei X, Huang Z, Zhong J (2014) Synthesis of CdS/ZnO/graphene composite with high-efficiency photoelectrochemical activities under solar radiation. Appl Surf Sci 299:12–18

Hasegawa G, Morisato K, Kanamori K, Nakanishi K (2011) New hierarchically porous titania monoliths for chromatographic separation media. J Sep Sci 34:3004–3010

He X, Chiu C, Esmacher MJ, Liang H (2013) Nanostructured photocatalytic coatings for corrosion protection and surface repair. Surf Coat Technol 237:320–327

Honda K, Fujishima A (1972) Electrochemical photolysis of water at a semiconductor electrode. Nature 238:37–38

Hong SJ, Jun H, Borse PH, Lee JS (2009) Size effects of WO_3 nanocrystals for photooxidation of water in particulate suspension and photoelectrochemical film systems. Int J Hydrogen Energy 34:3234–3242

Jaimy KB, Ghosh S, Sankar S, Warrier KGK (2011) An aqueous sol-gel synthesis of chromium (III) doped mesoporous titanium dioxide for visible light photocatalysis. Mater Res Bull 46:914–921

Jana TK, Pal A, Chatterjee K (2014) Self assembled flower like CdS–ZnO nanocomposite and its photo catalytic activity. J Alloys Compd 583:510–515

Jiang H, Wang Q, Zang S, Li J, Wang X (2014) Hydrothermal synthesis of high-efficiency Pr, N, P-tridoped TiO_2 from $TiCl_4$ hydrolysis and mechanism of its enhanced photoactivity. J Alloys Compd 600:34–42

Jindal K, Tomar M, Gupta V (2013) Nitrogen-doped zinc oxide thin films biosensor for determination of uric acid. Analyst 138:4353–4362

Kamat P (1997) Native and surface modified semiconductor nanoclusters, Progress in inorganic chemistry. In: Karlin D (ed) Progress in Inorganic Chemistry: Molecular Level Artificial Photosynthetic Materials, vol 44. John Wiley and Son, Hoboken, NJ, pp 273–343. ISBN ISBN 0-471-12535-0

Kato H, Hori M, Konta R, Shimodaira Y, Kudo A (2004) Construction of Z-scheme type heterogeneous photocatalysis systems for water splitting into H_2 and O_2 under visible light irradiation. Chem Lett 33:1348–1349

Kaur S, Singh V (2007) Visible light induced sonophotocatalytic degradation of Reactive Red dye 198 using dye sensitized TiO_2. Ultrason Sonochem 14:531–537

Khatamian M, Khandar AA, Divband B, Haghighi M, Ebrahimiasl S (2012) Heterogeneous photocatalytic degradation of 4-nitrophenol in aqueous suspension by Ln (La^{3+}, Nd^{3+} or Sm^{3+}) doped ZnO nanoparticles. J Mol Catal A Chem 365:120–127

Kohtani S, Kudo A, Sakata T (1993) Spectral sensitization of a TiO_2 semiconductor electrode by CdS microcrystals and its photoelectrochemical properties. Chem Phys Lett 206:166–170

Kominami H, Kato J, Murakami S, Ishii Y, Kohno M, Yabutani K, Yamamoto T, Kera Y, Inoue M, Inui T, Ohtani B (2003) Solvothermal syntheses of semiconductor photocatalysts of ultra-high activities. Catal Today 84:181–189

Konta R, Kato H, Kobayashi H, Kudo A (2003) Photophysical properties and photocatalytic activities under visible light irradiation of silver vanadates. Phys Chem Chem Phys 5:3061–3065

Kudo A, Omori K, Kato H (1999) A novel aqueous process for preparation of crystal form-controlled and highly crystalline $BiVO_4$ powder from layered vanadates at room temperature and its photocatalytic and photophysical properties. J Am Chem Soc 121:11459–11467

Kumara GRA, Kaneko S, Okuya M, Onwona-Agyeman B, Konno A, Tennakone K (2006) Shiso leaf pigments for dye-sensitized solid-state solar cell. Sol Energy Mat Sol C 90:1220–1226

Lehr D, Luka M, Wagner MR, Bügler M, Hoffmann A, Polarz S (2012) Band gap engineering of zinc oxide colloids via lattice substitution with sulfur leading to materials with advanced properties for optical applications like full inorganic UV protection. Chem Mater 24:1771–1778

Li X, Kikugawa N, Ye J (2008) Nitrogen-doped lamellar niobic acid with visible light responsive photocatalytic activity. Adv Mater 20:3816–3819

Li K, Yang C, Xu Y, Ying D, Wanga Y, Jia J (2012) Effect of inorganic anions on Rhodamine B removal under visible light irradiation using Bi_2O_3/Ti rotating disk reactor. Chem Eng J 211–212:208–221

Li D, Huang JF, Cao LY, Ll JY, OuYang HB, Yao CY (2014a) Microwave hydrothermal synthesis of Sr^{2+} doped ZnO crystallites with enhanced photocatalytic properties. Ceram Int 40:2647–2653

Li T, Chen Y, Fu WF (2014b) Photocatalytic H_2 production from water based on platinum (II) Schiff base sensitizers and a molecular cobalt catalyst. Catal Commun 45:91–94

Li Z, Shen Y, Guan Y, Hu Y, Lin Y, Nan CW (2014c) Bandgap engineering and enhanced interface coupling of graphene–$BiFeO_3$ nanocomposites as efficient photocatalysts under visible light. J Mater Chem A 2:1967–1973

Liu H, Peng T, Xiao J, Zhao D, Peng Z (2005) Preparation and photocatalytic activity of nanoscale Tb^{3+}-doped WO_3. J Wuhan Univ (Mater Sci Ed) 4:397–401

Liu H, Peng T, Ke D, Peng Z, Yan C (2007) Preparation and photocatalytic activity of dysprosium doped tungsten trioxide nanoparticles. Mater Chem Phys 104:377–383

Liu S, Yin K, Ren W, Cheng B, Yu J (2012) Tandem photocatalytic oxidation of Rhodamine B over surface fluorinated bismuth vanadate crystals. J Mater Chem 22:17759–17767

Liu L, Lv J, Xu G, Wang Y, Xie K, Chen Z, Wu Y (2013) Uniformly dispersed CdS nanoparticles sensitized TiO_2 nanotube arrays with enhanced visible-light photocatalytic activity and stability. J Solid State Chem 208:27–34

Lopes OF, Paris EC, Ribeiro C (2014) Synthesis of Nb_2O_5 nanoparticles through the oxidant peroxide method applied to organic pollutant photodegradation: A mechanistic study. Appl Catal B Environ 144:800–808

Maia DLS, Pepe I, Ferreira da Silva A, Silva LA (2012) Visible-light-driven photocatalytic hydrogen production over dye-sensitized β-$BiTaO_4$. J Photochem Photobiol A:Chem 243:61–64

Malato S, Fernández-Ibánez P, Maldonado MI, Blanco J, Gernjak W (2009) Decontamination and disinfection of water by solar photocatalysis: Recent overview and trends. Catal Today 147:1–59

Marschall R, Wang L (2014) Non-metal doping of transition metal oxides for visible light photocatalysis. Catal Today 225:111–135

Meyer BK, Polity A, Farangis B, He Y, Hasselkamp D, Krämer T, Wang C (2004) Structural properties and bandgap bowing of ZnO_{1-x} S_x thin films deposited by reactive sputtering. Appl Phys Lett 85:4929–4931

Mi Q, Ping Y, Li Y, Cao B, Brunschwig BS, Khalifah PG, Galli GA, Gray HB, Lewis NS (2012) Thermally stable N_2-intercalated WO_3 photoanodes for water oxidation. J Am Chem Soc 134:18318–18324

Min Y, Zhang K, Chen Y, Zhang YG, Zhao W (2012) Synthesis of nanostructured ZnO/Bi_2WO_6 heterojunction for photocatalysis application. Sep Purif Technol 92:115–120

Murase T, Irie H, Hashimoto K (2004) Visible light sensitive photocatalysts, nitrogen-doped Ta_2O_5 powders. J Phys Chem B 108:15803–15807

Nakata K, Fujishima A (2012) TiO_2 photocatalysis: design and applications. J Photochem Photobiol C 13:169–189

Narayan MR (2012) Review: Dye sensitized solar cells based on natural photosensitizers. Renewable Sustainable Energy Rev 16:208–215

Nozik AJ, Beard MC, Luther JM, Law M, Ellingson RJ, Johnson JC (2010) Semiconductor quantum dots and quantum dot arrays and applications of multiple exciton generation to third-generation photovoltaic solar cells. Chem Rev 110:6873–6890

O'Regan B, Grätzel M (1991) A low-cost, high-efficiency solar cell based on dye-sensitized colloidal TiO_2 films. Nature 353:737–740

Omidi A, Habibi-Yangjeh A, Pirhashemi M (2013) Application of ultrasonic irradiation method for preparation of ZnO nanostructures doped with Sb^{+3} ions as a highly efficient photocatalyst. Appl Surf Sci 276:468–475

Patil A, Patil K, Pardeshi S (2010) Ecofriendly synthesis and solar photocatalytic activity of S-doped ZnO. J Hazard Mater 183:315–323

Pei D, Luan J (2012) Development of visible light-responsive sensitized photocatalysts. Int J Photoenergy ID 262831:13

Persson C, Platzer-Bjorkman C, Malmstrom J, Torndahl T, Edoff M (2006) Strong valence band offset bowing of $ZnO_{1-x}S_x$ enhances p-type nitrogen doping of ZnO like alloys. Phys Rev Lett 97:146403

Phuruangrat A, Yayapao O, Thongtem T, Thongtem S (2014) Preparation, characterization and photocatalytic properties of Ho doped ZnO nanostructures synthesized by sonochemical method. Superlattices Microstruct 67:118–126

Radecka M, Sobas P, Wierzbicka M, Rekas M (2005) Photoelectrochemical properties of undoped and Ti-doped WO_3. Physica B 364:85–92

Rengifo-Herrera JA, Mielczarski E, Mielczarski J, Castillo NC, Kiwi J, Pulgarin C (2008) Escherichia coli inactivation by N, S co-doped commercial TiO_2 powders under UV and visible light. Appl Catal B Environ 84:448–456

Ropero-Vega JL, Rosas-Barrera KL, Pedraza-Avella JA, Laverde-Cataño DA, Pedraza-Rosas JE, Niño-Gómez ME (2010) Photophysical and photocatalytic properties of Bi_2MNbO_7 (M = Al, In, Ga, Fe) thin films prepared by dip-coating. Mater Sci Eng B 174:196–199

San Esteban ACM, Enriquez EP (2013) Graphene-anthocyanin mixture as photosensitizer for dye-sensitized solar cell. Sol Energy 98:392–399

Saravanakumar B, Mohan R, Thiyagarajan K, Kim SJ (2013) Investigation of UV photoresponse property of Al, N co-doped ZnO film. J Alloys Compd 580:538–543

Sayama K, Arakawa H (1994) Effect of Na_2CO_3 addition on photocatalytic decomposition of liquid water over various semiconductor catalysis. J Photochem Photobiol A:Chem 77:243–247

Shang M, Wang W, Sun S, Zhou L, Zhang L (2008) Bi_2WO_6 nanocrystals with high photocatalytic activities under visible light. J Phys Chem C 112:10407–10411

Sreethawong T, Yoshikawa S (2012) Impact of photochemically deposited monometallic Pt and bimetallic Pt-Au nanoparticles on photocatalytic dye-sensitized H_2 production activity of mesoporous-assembled TiO_2-SiO_2 mixed oxide nanocrystal. Chem Eng J 197:272–282

Sun T, Liu E, Fan J, Hu X, Wu F, Hou W, Yang Y, Kang L (2013) High photocatalytic activity of hydrogen production from water over Fe doped and Ag deposited anatase TiO_2 catalyst synthesized by solvothermal method. Chem Eng J 228:896–906

Takeuchi M, Shimizu Y, Yamagawa H, Nakamuro T, Anpo M (2011) Preparation of the visible light responsive N^{3-}-doped WO_3 photocatalyst by a thermal decomposition of ammonium paratungstate. Appl Catal B:Environ 110:1–5

Takizawa T, Watanabe T, Honda K (1978) Photocatalysis through excitation of adsorbates. 2. A comparative study of Rhodamine B and methylene blue on cadmium sulfide. J Phys Chem 82:1391–1396

Tanasa DE, Piuleac CG, Curteanu S, Popovici E (2013) Photodegradation process of Eosin Y using ZnO/SnO_2 nanocomposites as photocatalysts: experimental study and neural network modeling. J Mater Sci 48:8029–8040

Tang JW, Wang DF, Zou ZG, Ye JH (2003) Modification of photophysical properties of WO_3 by doping different metals. Mater Sci Forum 423–424:163–166

Thankalekshmi RR, Rastogi AC (2012) Structure and optical band gap of $ZnO_{12x}S_x$ thin films synthesized by chemical spray pyrolysis for application in solar cells. J Appl Phys 112: 063708-063708-10

Tuomisto F, Rauch C, Wagner MR, Hoffmann A, Eisermann S, Meyer BK, Kilanski L, Tarun MC, McCluskey MD (2013) Nitrogen and vacancy clusters in ZnO. J Mater Res 28:1977–1983

Tuzemen ES, Kara K, Elagoz S, Takci DK, Altuntas I, Esen R (2014) Structural and electrical properties of nitrogen-doped ZnO thin films. Appl Surf Sci http://dx.doi.org 10.1016/j.apsusc.2014.02.118

Ullah R, Sun H, Ang HM, Tade MO, Wang S (2013) Comparative investigation of photocatalytic degradation of toluene on nitrogen doped Ta_2O_5 and Nb_2O_5 nanoparticles. Ind Eng Chem Res 52:3320–3328

Vinodgopal K, Kamat P (1995) Enhanced rates of photocatalytic degradation of an azo dye using SnO_2/TiO_2 coupled semiconductor thin films. Environ Sci Technol 29:841–845

Vo V, Thi TPT, Kim HY, Kim SJ (2014) Facile post-synthesis and photocatalytic activity of N-doped ZnO–SBA-15. J Phys Chem Solids 75:403–409

Wang C, Cao L (2011) Preparation, spectral characteristics and photocatalytic activity of Eu^{3+}-doped WO_3 nanoparticles. J Rare Earths 29:727–731

Wang M, Chen C, Zhao B, Zeng Q, He D (2013) Solvothermal synthesis of nanostructured TiO_2 photocatalyst in supercritical CO_2 fluids. Mater Lett 109:104–107

Wang Z, Wang ZW, Yue Y, Cao Y (2014) Preparation and properties of nitrogen doped p-type zinc oxide films by reactive magnetron sputtering. Vacuum 101:313–316

Whitehead K, Hedges JI (2005) Photodegradation and photosensitization of mycosporine-like amino acids. J Photochem Photobiol B 80:115–121

Wongcharee K, Meeyoo V, Chavadej S (2007) Dye-sensitized solar cell using natural dyes extracted from rosella and blue pea flowers. Sol Energy Mater Sol Cells 91:566–571

Xu H, Zhou YN, Lu F, Fu ZW (2011) Electrochemistry of $ZnO_{1-x}S_x$ thin film with lithium. J Electrochem Soc 158:A285–A290

Xu L, Shi W, Guan J (2012) Preparation of crystallized mesoporous CdS/Ta_2O_5 composite assisted by silica reinforcement for visible light photocatalytic hydrogen evolution. Catal Commun 25:54–58

Yang S, Gao L (2004) New method to prepare nitrogen-doped titanium dioxide and its photocatalytic activities irradiated by visible light. J Am Ceram Soc 87:1803–1805

Yayapao O, Thongtem S, Phuruangrat A, Thongtem T (2013a) Sonochemical synthesis, photocatalysis and photonic properties of 3 % Ce-doped ZnO nanoneedles. Ceram Int 39: S563–S568

Yayapao O, Thongtem T, Phuruangrat A, Thongtem S (2013b) Ultrasonic-assisted synthesis of Nd-doped ZnO for photocatalysis. Mater Lett 90:83–86

Yoo YZ, Jin ZW, Chikyow T, Fukumura T, Kawasaki M, Koinuma H (2002) S doping in ZnO film by supplying ZnS species with pulsed laser deposition methods. Appl Phys Lett 81:3798–3790

Yu J, Dai G, Cheng B (2010) Effect of crystallization methods on morphology and photocatalytic activity of anodized TiO_2 nanotube array films. J Phys Chem C 114:19378–19385

Yun HJ, Lee H, Joo JB, Kim W, Yi J (2009) Influence of aspect ratio of TiO_2 nanorods on the photocatalytic decomposition of formic acid. J Phys Chem C 113:3050–3055

Zhang L, Fu H, Zhang C, Zhu Y (2006) Synthesis, characterization, and photocatalytic properties of $InVO_4$ nanoparticles. J Solid State Chem 179:804–811

Zhang D, Gong J, Ma JJ, Han G, Tong Z (2013) A facile method for synthesis of N-doped ZnO mesoporous nanospheres and enhanced photocatalytic activity. Dalton Trans 42:16556–16561

Zhang X, Wang DK, Schmeda López DR, Diniz da Costa JC (2014) Fabrication of nanostructured TiO_2 hollow fiber photocatalytic membrane and application for wastewater treatment. Chem Eng J 236:314–322

Zhao Z, Dai H, Deng J, Liu Y, Au CT (2013) Enhanced visible-light photocatalytic activities of porous olive-shaped sulfur-doped $BiVO_4$-supported cobalt oxides. Solid State Sci 18:98–104

Zheng YZ, Tao X, Hou Q, Wang DT, Zhou WL, Chen JF (2011) Iodine-doped ZnO nanocrystalline aggregates for Improved dye-sensitized solar cells. Chem Mater 23:3–5

Zhou H, Wu L, Gao Y, Ma T (2011) Dye-sensitized solar cells using 20 natural dyes as sensitizers. J Photochem Photobiol A:Chem 219:188–194

Zhu S, Fu H, Zhang S, Zhang L, Zhu Y (2008) Two-step synthesis of a novel visible-light-driven $K_2Ta_2O_{6-x}N_x$ catalyst for the pollutant decomposition. J Photochem Photobiol A 193:33–41

Zong X, Sun C, Yu H, Chen ZG, Xing Z, Ye D, Lu GQ, Li X, Wang L (2013) Activation of photocatalytic water oxidation on N-doped ZnO bundle-like nanoparticles under visible light. J Phys Chem C 117:4937–4942

Zou L, Liu Q, Xu Q, Mi G (2011) Microwave synthesis of mesoporous WO_3 doping with bismuth and photocatalytic oxidation of water to H_2. Korean J Chem Eng 28:1299–1303

http://www.springer.com/978-3-319-10998-5

Photocatalytic Semiconductors
Synthesis, Characterization, and Environmental Applications
Hernández-Ramírez, A.; Medina-Ramirez, I. (Eds.)
2015, XII, 289 p. 117 illus., 44 illus. in color., Hardcover
ISBN: 978-3-319-10998-5